Physics of the Earth and Planetary Interiors 183 (2010) 229–233

Contents lists available at ScienceDirect

Physics of the Earth and Planetary Interiors

journal homepage: www.elsevier.com/locate/pepi

Thermal diffusivity, thermal conductivity and heat capacity of serpentine (antigorite) under high pressure

M. Osako[a,*], A. Yoneda[b], E. Ito[b]

[a] Division of Physical Sciences, National Museum of Nature and Science, 3-23-1, Hyakunincho, Shinjuku-ku, Tokyo 169-0073, Japan
[b] Institute for Study of the Earth's Interior, Okayama University, Misasa, Tottori 682-0193, Japan

ARTICLE INFO

Article history:
Received 1 September 2009
Received in revised form 18 February 2010
Accepted 14 July 2010

Guest Editors
Daisuke Suetsugu
Craig Bina
Toru Inoue
Douglas Wiens

Editor
Mark Jellinek

Keywords:
Thermal conductivity
Thermal diffusivity
Heat capacity
Serpentine
Subduction zone

ABSTRACT

Thermal diffusivity and thermal conductivity of serpentine (antigorite) were measured up to 8.5 GPa and 800 K in the Kawai-type high-pressure apparatus. Antigorite has thermal diffusivity of 0.90×10^{-6} m^2 s^{-1} and thermal conductivity of 2.7 W m^{-1} K^{-1} at 5 GPa and 300 K, which are much lower than those of olivine. Furthermore, the pressure derivatives of thermal diffusivity and thermal conductivity are significantly smaller than those of olivine. The thermal properties of antigorite obtained in the present study imply existence of a thermal insulating layer in subduction zones. From the simultaneous measurement of both thermal diffusivity and thermal conductivity the heat capacity of antigorite was determined to be $\approx 1 \times 10^3$ J kg^{-1} K^{-1}, and increased to $\approx 1.5 \times 10^3$ J kg^{-1} K^{-1} at ≈800 K under high pressure. The heat capacity was nearly independent of pressure, which indicates nearly temperature-independent thermal expansivity of antigorite. Its characteristics also were hypothesized in terms of lattice dynamics of hydrous minerals involving hydrogen atoms and hydroxyl groups.

1. Introduction

Antigorite is a serpentine mineral ($Mg_6Si_4O_{10}(OH)_8$) of high-temperature form having a large wavy structure, and has been thought to be distributed extensively in the mantle wedge, where dehydrated water from the slab can infiltrate into the peridotite layer to produce serpentinite (Hyndman and Peacock, 2003). Its stability has been frequently investigated (e.g., Bose and Ganguly, 1995; Ulmer and Trommsdorff, 1995; Wunder and Schreyer, 1997; Irifune et al., 1998; Bromiley and Pawley, 2003; Hilairet et al., 2006a), such that the stability field has been determined to be limited to approximately <8 GPa and <1000 K.

Recently antigorite has been considered to be a kind of lubricant in the subduction process (Hilairet et al., 2007; Lee and Chen, 2007). The physical properties of antigorite have been studied extensively because it is a key material for understanding slab subduction, and for relating seismic and volcanic processes (e.g., Hilairet et al., 2006b; Reynard et al., 2007; Watanabe et al., 2007). Many seismological observations and geological processes have been interpreted in relation to serpentine (e.g., Rüpke et al., 2004; Kawakatsu and Watada, 2007). For instance, Katayama et al. (2009) attributed the alignment of antigorite in the hydrated mantle wedge as the source of seismic wave anisotropy observed in the warm portions of a subduction zone. Furthermore, its dehydration can be assigned as a trigger of earthquakes in downgoing slabs (e.g., Peacock, 2001; Omori et al., 2004).

Since the hydration and dehydration of the subduction zone is controlled by the temperature of the slab, the thermal conductivity of antigorite is an important factor in the temperature distribution and dehydration sequence in the slab. Although Horai (1971) measured thermal conductivity of serpentine polymorphs, his data were limited to ambient conditions. Thus, we determined thermal properties of antigorite including heat capacity under high pressure up to 8.5 GPa and at high temperature up to 820 K.

2. Experimental

The experiments were conducted by means of the pulse-heating method (Osako et al., 2004) in the Kawai-type apparatus (USSA-1000) at the Institute for Study of the Earth's Interior, Misasa, Japan.

* Corresponding author. Tel.: +81 3 5332 7174; fax: +81 3 3364 7104.
E-mail address: sako@kahaku.go.jp (M. Osako).

0031-9201/$ – see front matter © 2010 Elsevier B.V. All rights reserved.
doi:10.1016/j.pepi.2010.07.005

Table 1
Summary of P wave velocity measurement (km/s) under ambient conditions. Four specimens (≈2.4 mm × 2.7 mm × 4.0 mm) were prepared. Numbers 1–4 denote the different specimens. The *X*, *Y*, *Z* directions are specified arbitrarily, but they are perpendicular to each other and homogeneous among specimens. Note that the mean of "average" is 6.66 km/s. Measurements were conducted by using a 20 MHz P wave transducer.

	1	2	3	4	Average
X	6.79	6.87	6.79	6.81	6.82
Y	6.58	6.63	6.65	6.64	6.62
Z	6.48	6.48	6.68	6.58	6.55

The present method enables us to measure thermal diffusivity and thermal conductivity simultaneously. Thermal diffusivity, κ and thermal conductivity, λ, are related to one another as follows:

$$\kappa = \frac{\lambda}{\rho C} \quad (1)$$

where ρ is density and C is heat capacity. Therefore, we can evaluate the heat capacity of antigorite as well, as long as we can estimate ρ independently. The reliability of heat capacity measurement through κ and λ also was evaluated throughout by means of the finite element method (Yoneda et al., 2009). The outline of the method and the sample assembly are summarized in Appendix A.

The antigorite sample used in this study was from China; however, the exact location is unknown. The sample is of gem quality, with macroscopically homogeneous and isotropic appearance, although microscopic observations show slight differences in texture on three rectangular planes of the specimen. It is of light green color and transparent in thin section. Its nominal density of $2.585(3) \times 10^3$ kg/m^3 is 2.0% lower than the X-ray density of 2.638×10^3 kg/m^3 (estimated from Hilairet et al., 2006b). EDS analysis yielded an atomic composition of Mg/Si = 1.418 and Fe/Si = 0.010, indicating a formula of $(Mg_{5.67}Fe_{0.04})_{\Sigma=5.71}Si_4O_{10}(OH)_{7.42}$.

To confirm its isotropy as a bulk sample, we conducted ultrasonic velocity measurement on three different directions perpendicular to each other (Table 1) by using the 20 MHz carrier wave. Results supported "isotropic assumption" within 5% P wave velocity fluctuation. Furthermore, X-ray diffraction in the three perpendicular planes did not show any significant difference in the profile. Therefore, we conducted measurements on a single direction.

In addition, the sample V_p of 6.66 km/s is higher than the estimated value of 6.52 km/s from seismological study at the ≈1 Hz frequency range (Christensen, 2004). It is not known if the difference in density between the nominal and the X-ray estimate of 2.0% can be entirely attributed to the porosity of the sample. If so, the intrinsic V_p of antigorite must be significantly higher than known so far. Since elastic wave velocity is not the focus of the present study, we only point out that: (1) a higher velocity value should be used in interpretation of seismological observations; or (2) substantial velocity dispersion is expected in antigorite between ≈1 Hz and 20 MHz owing to significant attenuation loss of wave energy. Hence, we were unable to measure S wave velocity owing to this enormous attenuation.

3. Results and discussion

Fig. 1 shows pressure effects in thermal diffusivity and thermal conductivity of antigorite. Changes in sample size by compression were corrected by assuming 60 GPa for the bulk modulus and 4.0 for its pressure derivative, although compressibility of antigorite is still controversial (Hilairet et al., 2006b). The pressure derivatives of κ and λ are much smaller than those for olivine up to 5 GPa. Above 5 GPa, they both decrease to nearly zero or indicate a slightly negative derivative on pressure. Therefore, we tried two types of

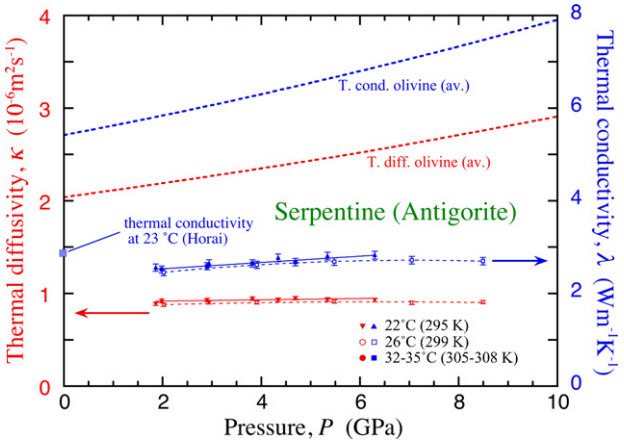

Fig. 1. Pressure dependence of thermal diffusivity, κ, and thermal conductivity, λ, of antigorite up to 8.5 GPa at ambient temperatures. Note the small bars for each data point, which indicate experimental errors. Small temperature fluctuations (22–35 °C) reflect seasonal and daily temperature variations. Thermal conductivity of antigorite at ambient conditions (Horai, 1971) is shown as well. The upper broken lines are thermal diffusivity and thermal conductivity of olivine (Osako et al., 2004) for comparison.

curve fitting; one is a linear fit to ≈6 GPa for set of three runs.

$$\kappa = 0.91 + 0.007 \times P \quad (2)$$

$$\lambda = 2.40 + 0.07 \times P \quad (3)$$

and the other a square fitting for 299 K data to 8.5 GPa.

$$\kappa = 0.84 + 0.021 \times P - 0.0017 \times P^2 \quad (4)$$

$$\lambda = 2.21 + 0.142 \times P - 0.010 \times P^2 \quad (5)$$

where P is in GPa, κ in 10^{-6} m^2 s^{-1}, and λ in W m^{-1} K^{-1}. Our thermal conductivity data suggest smaller values than that at the ambient condition by Horai (1971) for natural antigorite produced in Vermont, USA. Although no details about Horai's sample are available, the difference may be attributed to the specimen variability in composition or texture used in the two studies. Furthermore, it is noted that the density of Horai's sample (2.656×10^3 kg/m^3) was 2.7% higher than that of the present sample.

Antigorite has much lower thermal diffusivity and thermal conductivity (less than half) of the major dry mantle minerals such as olivine. Through a simple evaluation, the thermal conductivity difference between olivine and antigorite (≈3 W m^{-1} K^{-1}) can yield a temperature gradient difference of ≈20 K/km under the assumption of typical earth's heat flow of 69×10^{-3} W m^{-2}. Katayama et al. (2009) estimated ≈20 km thickness of the serpentine layer for the Ryukyu subduction zone from seismological anisotropy study. Thus a ≈400 K temperature difference could be estimated for the thin layer if the constituting material is hydrated from peridotite to serpentinite. Katayama et al. (2009) also claims that the *c*-axis of antigorite (the slowest direction for S wave velocity in antigorite) tends to align normal to the plate interface. It may be reasonable to assume antigorite has low thermal conductivity along the *c*-axis. Therefore, even if other components in the serpentinite may reduce the effect of thermal insulation, the lattice preferred orientation of antigorite may still enhance the thermal insulation of the serpentinite layer. In the warm subduction zone, the serpentinite layer may act as an efficient thermal insulator for the subducting slab beneath it. In other words, the temperature increase of the slab is likely to be efficiently suppressed by the existence of the thermal insulating layer of serpentine.

In spite of the preliminary state, we measured thermal conductivity of talc as well, and obtained relatively higher thermal conductivity compared with antigorite. It is well known that antig-

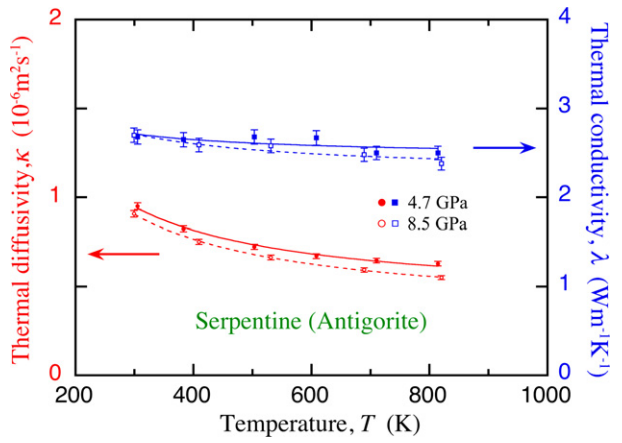

Fig. 2. Temperature dependence of thermal diffusivity, κ, and thermal conductivity, λ, of antigorite up to ≈800 K at 4.7 GPa and 8.5 GPa.

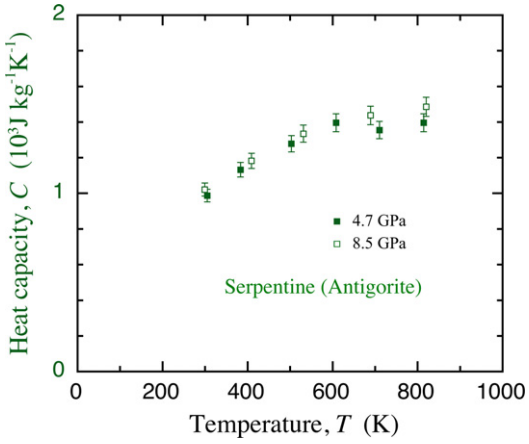

Fig. 3. Temperature dependence of heat capacity of antigorite.

orite and talc are quite similar hydrous sheet minerals. Although talc, the softest mineral in the Mohs hardness scale, has lower acoustic velocity than antigorite, thermal conductivity of talc is two to three times greater than that of antigorite (Yoneda et al., in preparation; Horai, 1971). This apparent contradiction may be attributed to antigorite's alternating wavy structure with a few nanometer wavelength (e.g., Watanabe et al., 2007). In terms of a simple calculation, phonons excited at ≈300 K tend to have wavelengths shorter than 1 nm. Therefore, phonons are expected to be trapped in a wavy segment of the antigorite crystal structure. This effect can cause lower thermal conductivity for antigorite.

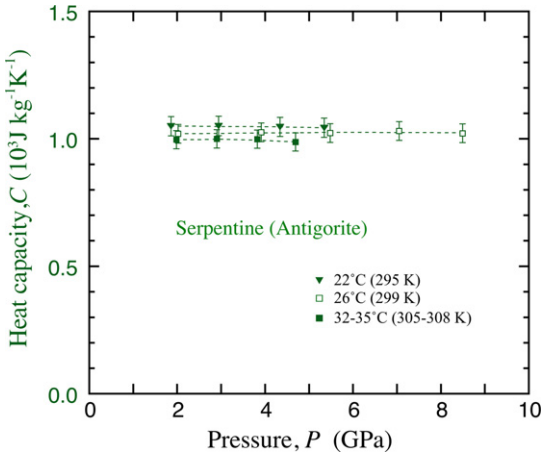

Fig. 4. Heat capacity of antigorite under high pressure and at ambient temperature.

Table 2
List of $\partial C_P/\partial P$ and $\partial\alpha/\partial T$ for the three minerals at 300 K. It is noted that we assumed 3000 kg/m^3 and 2.65×10^{-5} K^{-1} for ρ and α commonly in the derivation of $\partial\alpha/\partial T$ from $\partial C_P/\partial P$. The value of $\partial C_P/\partial P$ for olivine is the average of the measurements among the three crystallographic orientations in olivine (Osako et al., 2004).

	$\partial C_P/\partial P$	$\partial\alpha/\partial T$
Olivine	-3.3×10^{-9} J kg^{-1} K^{-1} Pa^{-1}	3.2×10^{-8}
Antigorite	≈0	-10^{-9}
Talc	30×10^{-9}	-3×10^{-7}

Fig. 2 shows the temperature dependence of thermal diffusivity and thermal conductivity of antigorite. Thermal diffusivity decreases faster than thermal conductivity, which indicates rapid increase of heat capacity with increasing temperature. We can recognize a pressure effect on thermal diffusivity at high temperature; thermal diffusivity at 8.5 GPa is slightly lower than that at 4.7 GPa. On the other hand, we cannot recognize a clear pressure effect on thermal conductivity within the margin of error. Although the temperature elevation at 8.5 GPa must cross the phase boundary of antigorite decomposition, a significant anomaly was not observed

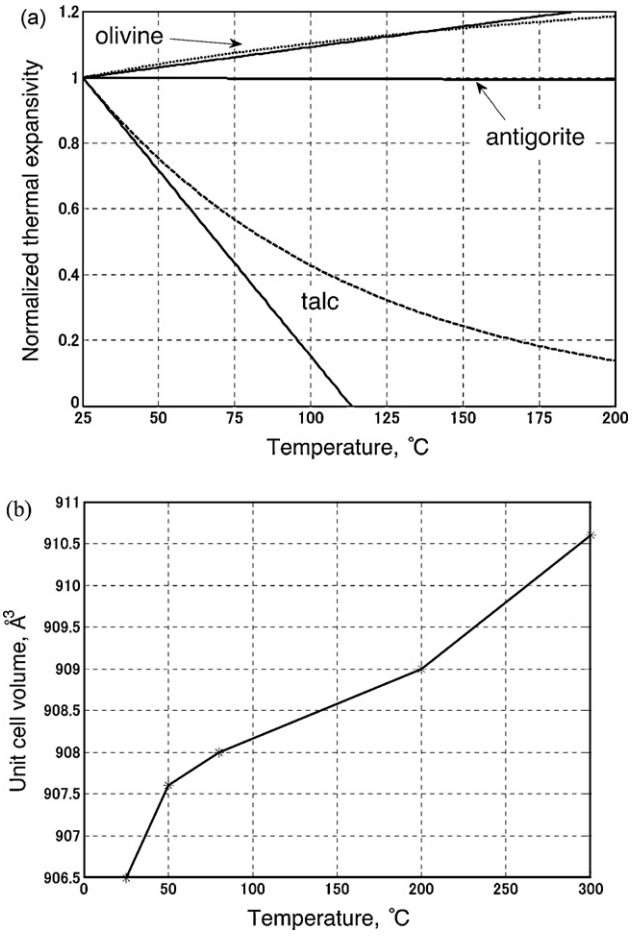

Fig. 5. (a) Estimation of temperature dependence of thermal expansivity for serpentine, olivine, and talc. Thermal expansivity is normalized by 2.65×10^{-5}, which is the experimental value for olivine at 25 °C (Suzuki, 1975). For evaluating the temperature variation shown by the solid lines, we assumed 2.65×10^{-5} typical for olivine, antigorite and talc as a representative value of thermal expansivity at 25 °C, and applied the temperature derivatives shown in Table 2. The dotted line for olivine is the experimental results for olivine (Suzuki, 1975). The dashed curve for talc is a realistic modification by considering the reported thermal expansion for talc, which did not show negative thermal expansivity (b), as shown by Pawley et al. (1995).

in the process of measurement of thermal diffusivity and thermal conductivity.

Fig. 3 shows temperature dependence of heat capacity of antigorite. Although the results show rapid increase of heat capacity, it is lower than the Dulong–Petit limit of C_V for antigorite (1.62×10^3 J kg^{-1} K^{-1}). Comparing the trend between 4.7 GPa and 8.5 GPa heating experiments, the scatter over 700 K for 4.7 GPa heating may correspond to some experimental problem.

Fig. 4 shows the heat capacity of antigorite at ambient temperature; it is $\approx 1.0 \times 10^3$ J kg^{-1} K^{-1} and nearly independent of pressure increase. The reproducibility among the three data types was as good as within ≈5%. The pressure derivative of heat capacity, $\partial C_P/\partial P$, of antigorite is nearly zero. This value contrasts with the negative value for olivine (Table 2). On the other hand, preliminary results for talc were as large as $\partial C_P/\partial P \approx +30$ J kg^{-1} K^{-1} GPa^{-1} (Yoneda et al., in preparation).

From the pressure derivatives of heat capacity, we can evaluate characteristics of the thermal expansivity, α, through the following thermodynamic identity:

$$\left(\frac{\partial C_P}{\partial P}\right)_T = -\frac{T}{\rho}\left[\alpha^2 + \left(\frac{\partial \alpha}{\partial T}\right)_P\right] \quad (6)$$

From the observation of pressure derivatives of heat capacity and typical thermal expansivity (2.65×10^{-5} K^{-1}; see Table 2), we can expect the temperature derivative of thermal expansivity for the three materials as shown in Table 2. Although reliable thermal expansion data are not available for antigorite, we demonstrate it together with those for olivine and talc in Fig. 5. If the negatively small $\partial\alpha/\partial T$ is exact, we can expect nearly constant thermal expansivity for antigorite. In other words, the volume of antigorite increases almost linearly with temperature.

From lattice dynamic theory, we can define the mode Grüneisen parameter, γ_i, for the normal mode of lattice vibration as:

$$\gamma_i = -\frac{\partial \log \omega_i}{\partial \log V} \quad (7)$$

where ω_i is the angular frequency of normal mode specified by the subscript "i", and V is volume (e.g., Kieffer, 1979). Note that positive γ_i contributes to positive thermal expansion, and vice versa. Thus, the majority of γ_i for olivine is expected to be positive, because the $\partial\alpha/\partial T$ for olivine is positive. On the other hand, some of the γ_i for antigorite and talc are expected to be negative because of the negative $\partial\alpha/\partial T$. It is quite probable that the hydrous mode, or normal mode related with hydrogen and hydroxyl groups, may have a negative mode Grüneisen parameter.

4. Conclusions

The low thermal conductivity of antigorite leads to the conclusion that there exists a thermal insulating layer where serpentinization arises in the subduction zone. In this case, the temperature in the layer is expected to be maintained lower than the surroundings, and the unstable antigorite can intrude into deeper areas, crossing the dehydration boundary owing to the lower kinetics of low temperature. It is noteworthy that a sudden dehydration from unstable antigorite is one of the possible triggers of the intermediate-depth (50–130 km) earthquakes (Perrillat et al., 2005).

The present study provides the first set of simultaneous measurements of thermal diffusivity and thermal conductivity of hydrous silicate minerals under high pressure. Consequently, these are pioneering heat capacity data for hydrous minerals. One of the pronounced results is that the data predict nearly temperature-independent thermal expansivity for antigorite.

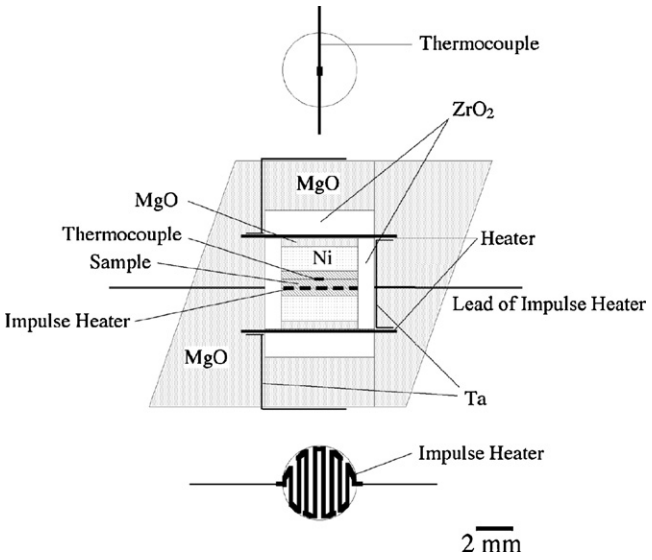

Fig. A1. Cross-section of the sample assembly. Top views of the thermocouple and impulse heater are also shown. The flat chromel–alumel thermocouple has a thickness of 0.03 mm and a width of 0.3 mm, and the impulse heater has a thickness of 0.03 mm. Although the circuit pattern of the nickel–chromium impulse heater (3.8 mm in diameter and 0.03 mm in thickness) is shown schematically, the striped pattern of the impulse heater circuit is actually folded 20 times.

Acknowledgments

The authors thank K. Yokoyama, M. Shigeoka, and T. Tsujimori for characterization of the sample, and T. Maeda and C. Oka for assistance with the high-pressure experiment. We acknowledge two anonymous reviewers for their helpful comments which improved the manuscript. This work was supported by a Grant in Aid for Scientific Research (No. 17037005) in the "Stagnant slab" project sponsored by MEXT. It was also carried out as joint research in the Institute for Study of the Earth's Interior, Okayama University.

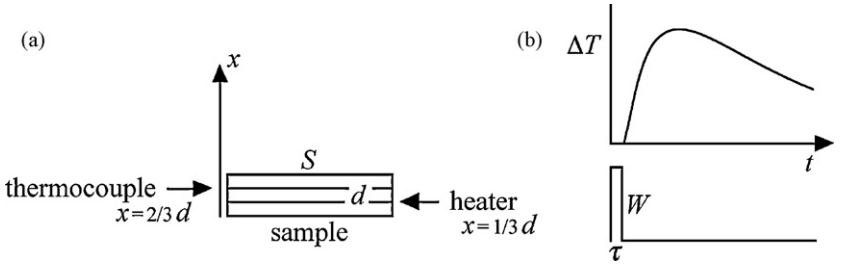

Fig. A2. The concept of the sample assembly and measurement of a pulse-heating method for measurement of thermal conductivity/diffusivity from Dzhavadov (1975). (a) Illustration of the basic configuration of the sample. d is the total height of the three sample disks, S is the area of the heater, and x is the position from the bottom of the sample (the heater is at $x = d/3$ and the thermocouple is at $x = 2d/3$). The temperature change ΔT caused by impulse heating with a power of W is monitored by the thermocouple (b), where τ is the duration of pulse heating and t is time from the onset of heating.

Appendix A. Brief summary of thermal conductivity/diffusivity measurement

Fig. A1 shows the cell assembly and Fig. A2 the basic concept of the experimental technique used in this study. The sample consists of three thin identical disks. An impulse heater is placed at one interface between the disks, and a thermocouple is inserted at the other interface. The thermal disturbance caused by impulse heating is monitored by the thermocouple.

The acquired data are analyzed based on an explicit equation solved under the assumption of one-dimensional heat flow and constant temperature boundary conditions (Dzhavadov, 1975):

$$\Delta T = A\sum_{n=1}^{\infty}\frac{1}{n^2}\sin\frac{n\pi}{3}\sin\frac{n\pi x}{d}\exp(-n^2Bt)[\exp(n^2B\tau)-1] : (t>\tau) \tag{A1}$$

where t is time from the onset of heating, x is the position measured from the end of the sample, d is the total height of the three sample disks, and τ is the duration of the heating pulse. The quantities A and B are defined as

$$A = \frac{2Wd}{\pi^2\lambda S}, \quad B = \frac{\pi^2\kappa}{d^2} \tag{A2}$$

where W is the power of the impulse heating and S is the area of the heater.

As the series in Eq. (A1) converges rapidly, summation to $n = 10$ yields a very accurate value, in comparing the calculation error with experimental uncertainty. The parameters A and B are determined through least square fitting of the experimental data by means of Eq. (A1) up to $n = 15$. By substituting A and B into Eq. (A2), λ and κ are obtained simultaneously.

References

Bose, K., Ganguly, J., 1995. Experimental and theoretical studies of the stabilities of talc, antigorite and phase A at high pressures with applications to subduction processes. Earth Planet. Sci. Lett. 136, 109–121.

Bromiley, G.D., Pawley, A.R., 2003. The stability of antigorite in the systems MgO–SiO–H_2O (MSH) and MgO–Al_2O_3–SiO–H_2O (MASH): the effects of Al^{3+} substitution on high-pressure stability. Am. Mineral. 88, 99–108.

Christensen, N.I., 2004. Serpentine, peridotites, and seismology. Int. Geol. Rev. 46, 795–816.

Dzhavadov, L.N., 1975. Measurement of thermophysical properties of dielectrics under pressure. High Temp.-High Press. 7, 49–54.

Hilairet, N., Daniel, I., Reynard, B., 2006a. *P–V* equations of state and the relative stabilities of serpentine varieties. Phys. Chem. Miner. 33, 629–637.

Hilairet, N., Daniel, I., Reynard, B., 2006b. Equation of state of antigorite, stability field of serpentines, and seismicity in subduction zones. Geophys. Res. Lett. 33, L02302, doi:10.1029/2005GL024728.

Hilairet, N., Reynard, B., Wang, Y., Daniel, I., Merkel, S., Nishiyama, N., Petitgirard, S., 2007. High-pressure creep of serpentine, interseismic deformation, and initiation of subduction. Science 318, 1910–1913.

Horai, K., 1971. Thermal conductivity of rock-forming minerals. J. Geophys. Res. 76, 1278–1308.

Hyndman, R.D., Peacock, S.M., 2003. Serpentinization of the forearc mantle. Earth Planet. Sci. Lett. 212, 417–432.

Irifune, T., Kubo, N., Issiki, M., Yamasaki, Y., 1998. Phase transformations in serpentine and transportation of water into the lower mantle. Geophys. Res. Lett. 25, 203–206.

Katayama, I., Hirauchi, K., Michibayashi, K., Ando, J., 2009. Trench-parallel anisotropy produced by serpentine deformation in the hydrated mantle wedge. Nature 461, 1114–1118.

Kawakatsu, H., Watada, S., 2007. Seismic evidence for deep-water transportation in the mantle. Science 316, 1468–1471.

Kieffer, S.W., 1979. Thermodynamics and lattice vibrations of minerals: 2. Vibrational characteristics of silicates. Rev. Geophys. Space Phys. 17, 20–34.

Lee, C.A.-T., Chen, W.-P., 2007. Possible density segregation of subducted oceanic lithosphere along a weak serpentinite layer and implications for compositional stratification of the Earth's mantle. Earth Planet. Sci. Lett. 255, 357–366.

Omori, S., Komabayashi, T., Maruyama, S., 2004. Dehydration and earthquake in the subducting slab: empirical link in intermediate and deep seismic zones. Phys. Earth Planet. Int. 146, 297–311.

Osako, M., Ito, E., Yoneda, A., 2004. Simultaneous measurements of thermal conductivity and thermal diffusivity for garnet and olivine under high pressure. Phys. Earth Planet. Int. 143–144, 311–320.

Pawley, A.R., Redfern, S.A.T., Wood, B.J., 1995. Thermal expansivities and compressibilities of hydrous phases in the system MgO–SiO_2–H_2O: talc, phase A and 10-Å Phase. Contrib. Mineral. Petrol. 122, 301–307.

Peacock, S.M., 2001. Are the lower planes of double seismic zones caused by serpentine dehydration in subducting oceanic mantle? Geology 29, 299–302.

Perrillat, J.-P., Daniel, I., Koga, K.T., Reynard, B., Cardon, H., Crichton, W.A., 2005. Kinetics of antigorite dehydration: a real-time X-ray diffraction study. Earth Planet. Sci. Lett. 236, 899–913.

Reynard, B., Hilairet, N., Balan, E., Lazzeri, M., 2007. Elasticity of serpentines and extensive serpentinization in subduction zones. Geophys. Res. Lett. 34, L13307, doi:10.1029/2007GL030176.

Rüpke, L.H., Morgan, J.P., Hort, M., Connolly, J.A.D., 2004. Serpentine and the subduction zone water cycle. Earth Planet. Sci. Lett. 223, 17–34.

Suzuki, I., 1975. Thermal expansion of periclase and olivine and their anharmonic properties. J. Phys. Earth 23, 145–159.

Ulmer, P., Trommsdorff, V., 1995. Serpentine stability to mantle depths and subduction-related magmatism. Science 268, 858–861.

Watanabe, T., Kasami, H., Ohshima, S., 2007. Compressional and shear wave velocities of serpentinized peridotites up to 200 MPa. Earth Planets Space 59, 233–244.

Wunder, B., Schreyer, W., 1997. Antigorite: high pressure stability in the system MgO–SiO–H_2O (MSH). Lithos 41, 213–227.

Yoneda, A., Osako, M., Ito, E., 2009. Heat capacity measurement under high pressure: a finite element method assessment. Phys. Earth Planet. Int. 174, 309–314.